IRAQI JOURNAL OF MATERIALS
Volume (2) Issue (1) January-March 2023, pp. 33-40

Emission Lines of Laser-Produced Plasmas of Metal Targets Using Optical Emission Spectroscopy

Abbas F. Mahood

Department of Physics, College of Science, University of Thi Qar, Nasiriyah, IRAQ

Abstract

In this work, emission lines of laser-produced plasmas from three different metallic targets (copper, titanium and nickel) were detected by the optical emission spectroscopy. These plasmas were generated by irradiation of the metallic target with laser pulses of high peak power in room environment. Both electron density and electron temperature were determined for the three targets at different peak laser powers using the ratios of line intensities based on the obtained emission spectra. Electron temperatures were determined in the range 0.34-0.442 eV for copper target at laser power of 70 MW, 0.281-0.418 eV for titanium target at laser power of 60 MW, and 0.35-0.46 eV for nickel target at laser power of 70 MW.

Keywords: Laser-produced plasma; Emission line; Electron density; Electron temperature
Received: 10 August 2022; **Revised:** 17 November; **Accepted:** 24 December; **Published:** 1 January 2023

1. Introduction

Pulsed-laser induced plasma of solids is the subject of investigation in many fields of applied research such as laser plasma sources to x-ray lasers, inertial confinement fusion and laboratory astrophysics [1-3]. A pulsed laser source is employed to vaporize and excite the analyte forming plasma [4]. The optical emission from the relaxation of excited species within the plasma yields information regarding the composition of the material under test [5-7]. The plasma and its characteristics (electron density, electron temperature, spatial and temporal behavior) depend on the target's thermophysical properties and laser beam parameters, such as laser pulse, temporal duration and shape, laser wavelength and energy [8-12]. Plasma descriptions start by trying to characterize the properties of the assembly of atoms, molecules, electrons and ions rather than the individual species [13]. If thermodynamic equilibrium exists, the plasma properties such as the description of the speed of the particles and the relative populations of energy level can be described through the concept of the temperature [14-17].

The electron temperature is an equally important plasma parameter which can be spectroscopically determined in a variety of ways: from the ratio of integrated line intensities, from the ratio of line intensity to underlying continuum and from the shape of the continuum spectrum [18-21]. The diagnostic techniques employed for the determination of electron density includes plasma spectroscopy, Langmiur probe, microwave and laser interferometry and Thomson scattering [22-24]. Spectroscopy technique is the simplest as far as instrumentation is concerned [25].

Laser-induced breakdown spectroscopy (LIBS) is a rapid chemical analysis technology that uses a short laser pulse to create a micro-plasma on the sample surface [26-28]. This analytical technique offers many compelling advantages compared to other elemental analysis techniques [29]. These include a sample preparation-free measurement experience, extremely fast measurement time (usually a few seconds) for a single spot analysis, broad elemental coverage, including lighter elements, such as H, Be, Li, C, N, O, Na, and Mg, versatile sampling protocols that include fast raster of the sample surface and depth profiling, and finally thin-sample analysis without the worry of the substrate interference [30-34]. A typical detection limit of LIBS for heavy metallic elements is in the low-ppm range [35]. LIBS is applicable to a wide range of sample matrices that include metals, semiconductors, glasses, biological tissues, insulators, plastics, soils, plants, soils, thin-paint coating, and electronic materials [36].

For LIBS, Echelle spectrographs are typically used. For analysis of a wide range of samples, a system based on an Echelle spectrograph offers a combination of high resolution and wide wavelength

coverage [37]. It is also possible to relay the laser light to the sample and collect the signal by fiber optics. The gating requirements of LIBS are not very demanding [38]. Gate times and delays of several microseconds are typical. The intensity of the plasma emission is usually high enough to allow good spectra to be recorded in single scan mode [39].

In this work, emission lines of laser-produced plasmas from three different metallic targets (copper, titanium and nickel) are detected by the optical emission spectroscopy. These plasmas are generated by irradiation of the metallic target with Nd:YAG laser pulses of high peak power in room environment. Both electron density and electron temperature are determined for the three targets at different peak laser powers using the ratios of line intensities based on the obtained emission spectra.

2. Experiment

The optical emission spectra of copper, titanium and nickel plasmas were recorded using the experimental setup of laser-induced breakdown spectroscopy (LIBS) shown in Fig. (1). It consists of pulsed Nd:YAG laser of 1064 nm wavelength, 9 ns duration, 1 Hz pulse repetition frequency and peak power up to 120 MW. The laser beam was focused on the surface of the irradiated sample located at the focal length of a converging lens (f=10cm). An optical fiber holding photodetector was adjusted at 45° with beam direction at 5 cm distance from the sample where plasma is generated. The emission from the tin plasma plume was recorded using Ocean Optics HR 4000 CG-UV-NIR spectrum analyzer in the spectral range 320-750 nm.

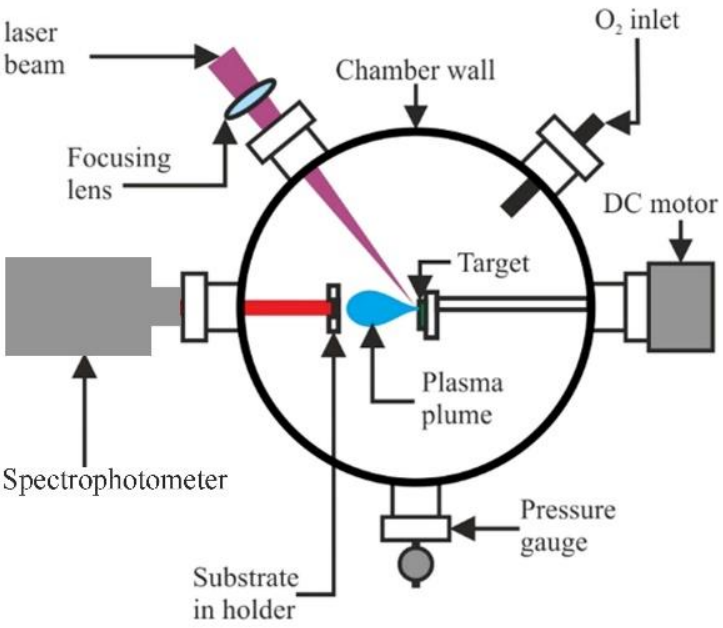

Fig. (1) The experimental setup for the laser-induced breakdown spectroscopy used in this work

3. Results and Discussion

The optical emission spectra of laser-produced plasmas of copper, titanium and nickel in the range 300-800 nm are shown in Fig. (2). The prominent spectral lines of copper target in room environment (Fig. 2a) are Cu I (421.2 nm), Cu II (642.5 nm) and Cu III (713.1 nm) in addition to other lines with low intensities those will be neglected when determining both electron density and electron temperature. Similarly, the prominent spectral lines of titanium target in room environment (Fig. 2b) are Ti I (414.3 nm), Ti II (635.6 nm) and Ti III (706.2 nm) in addition to other lines with low intensities those will be neglected too when determining both electron density and electron temperature. For nickel target, the prominent spectral lines in room environment (Fig. 2c) are Ni I (407.4 nm), Ni II (628.7 nm) and Ni III (699.3 nm) in addition to other lines with low intensities those will also be neglected when determining both electron density and electron temperature. The transitions are identified using the spectral database of National Institute of Standards and Technology (NIST) [21].

ISSN (print) 2958-8960 (online) xxxx-xxxx Printed in IRAQ

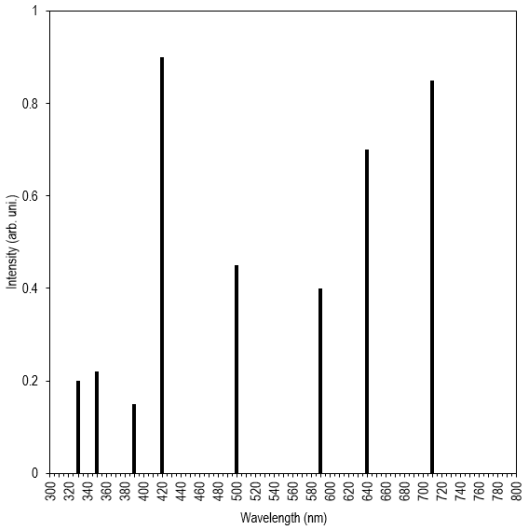

(a)

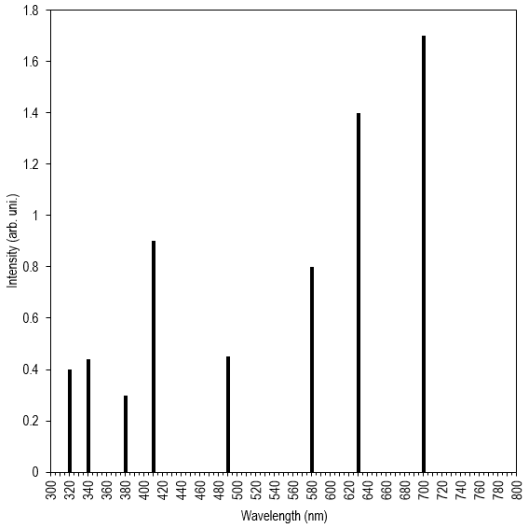

(b)

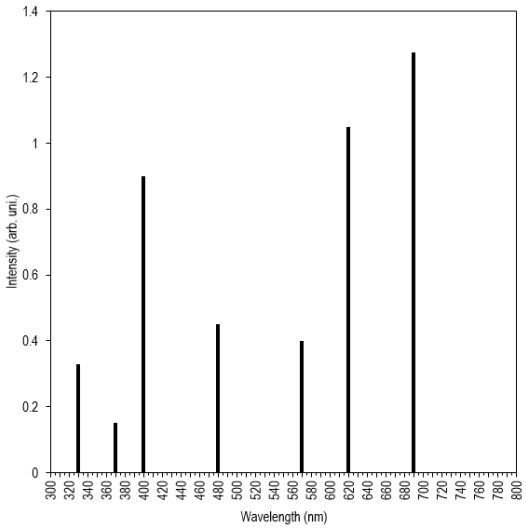

(c)

Fig. (2) Optical emission spectra of (a) copper, (b) titanium and (c) nickel plasmas produced by pulsed laser of 55 MW peak power

ISSN (print) 2958-8960 (online) xxxx-xxxx Printed in IRAQ

The intensities of copper plasma lines at 421.2, 642.5 and 713.1 nm were measured at different laser peak powers. Figure (3a) shows the influence of the laser peak power on the spectral line intensities. In similar manner, the intensities of titanium plasma lines at 414.3, 635.6 and 706.2 nm as well as the intensities of nickel plasma lines at 407.4, 628.7 and 699.3 nm were also measured at different laser peak powers, as in Fig. (3b) and (3c).

As shown, the emission intensity of the spectral lines increases with increasing laser peak power from 20 to 120 MW. This is due to the absorption of laser photon by the plasma and the plasma transparency to the laser beam. Therefore, the ablation of the metallic target increases [22]. Such increase produces a consequent increase in the height and emission of produced. At higher values of laser peak powers, plasma shielding effect is observed, i.e., the plasma becomes opaque to the laser beam which shields the target so the lines intensities decreases.

A major difference between the variations of line intensity with laser power for the three metallic targets can be seen in the full-width half maximum (FWHM). The emission spectra for copper target are reasonably narrower than those of titanium target. The FWHM for Cu III line is 48 nm while the FWHM for Ti III is 600 nm. For nickel target, the spectra are apparently wide enough to consider the determination of the FWHM. The highest intensities of the Ti III (706.2 nm) and Ni III (699.3 nm) are noticeably comparable but lower than that of Cu III (713.1 nm).

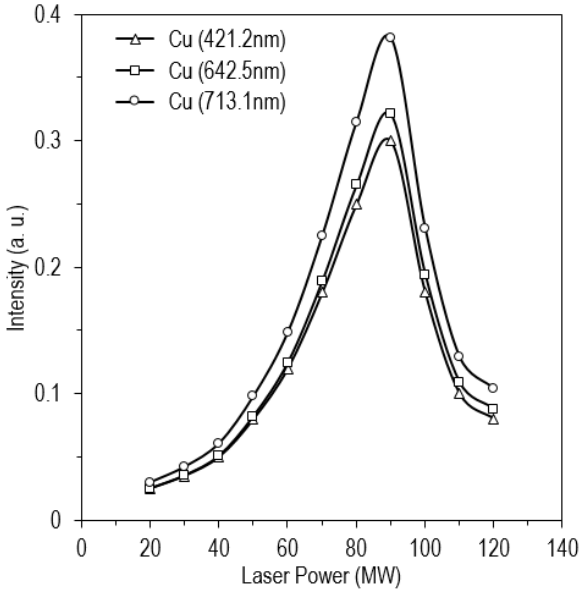

(a)

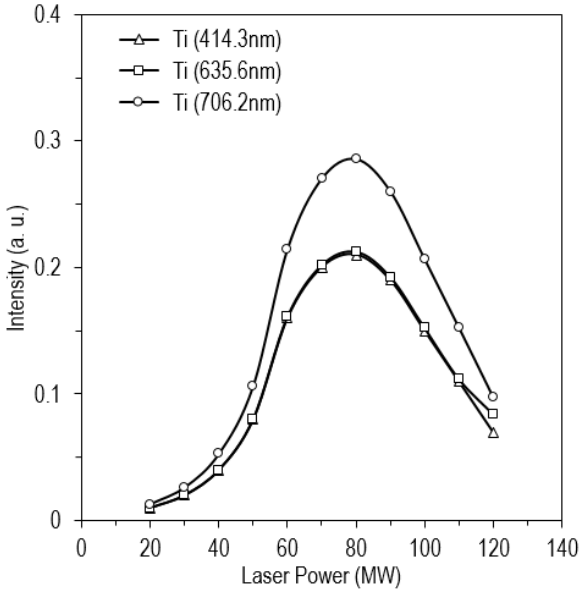

(b)

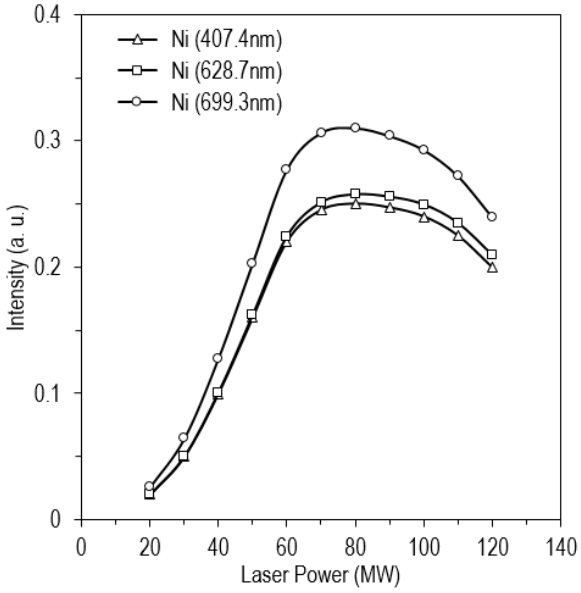

(c)

Fig. (3) Variation of emission intensity with laser peak power for the three metallic targets used in this work (a) copper, (b) titanium and (c) nickel

One of the important parameters for using optical spectroscopy for isotopic analysis is linewidth to line separation. Optical transitions, both atomic and molecular, are not immune to environmental factors and hence never provide precisely sharp line structures. While LA is a powerful technique for generating ions, atoms, and molecules from a solid material, the species are generated in a high-temperature and high-electron density environment. These conditions lead to significant spectral line broadening, which may reduce the ability to resolve small isotope splittings. Prominent broadening mechanisms that influence spectral linewidths in a laser-produced plasma are Doppler, pressure, and Stark effects. An in-depth knowledge of these line broadening mechanisms in a laser-produced plasma system is ultimately important to employ optical spectroscopy for isotopic analysis.

On the other hand, the intensities of nickel target lines at higher laser powers (>80 MW) are higher than those of copper and titanium at the same values of laser powers. These differences are related to the physical and chemical properties of these metals as the surface and environmental conditions are sufficiently kept the same.

Under the assumption that the plasma in local thermodynamic equilibrium (LTE), the lower limit of the electron density is given by [23]:

$$n_e \geq 1.6 \times 10^{12} \, (\Delta E)^3 \, (T_e)^{\frac{1}{2}} \qquad (1)$$

where n_e is the electron density, T_e is the electron temperature and ΔE is the energy difference between the states. The values of n_e are obtained from Saha-Boltzmann equation as [14]:

$$n_e = \frac{2(2\pi m_e k_B T_e)^{3/2}}{h^3} \frac{I^{I}_{mn} A_{ij} g^{II}_{i}}{I^{II}_{ij} A_{mn} g^{I}_{m}} e^{-\frac{E_{ion}+E^{II}_{i}-E^{I}_{m}}{k_B T_e}} \qquad (2)$$

where m_e is the electron mass, k_B is Boltzmann constant, *h* is Planck's constant and E_{ion} is the ionization potential of the neutral species in its ground state, I_{ji} is the intensity of the spectral line of the transition from level *j* to *i*, λ_{ji} is the wavelength, A_{ji} is the transition probability, g_j is the statistical weight, E_j is the energy value of higher level

Figure (4) shows the electron density of laser-induced plasmas of copper, titanium and nickel at different laser peak powers. It can be observed that for all the metallic targets, the electron density grows as the laser peak power is increased. The reason is that when a solid sample is irradiated by Nd:YAG laser pulses, a collision-induced process occurs and hence free electrons in the focal volume are accelerated by the electric field of the laser beam and gained energy by colliding with neutral atoms. When the electrons have gained amount of energy, they can ionize atoms by collision and this causes the electron density to grow with the laser peak power. The electron density dramatically decreases at high laser peak powers, this is due the plasma shielding as discussed previously.

The electron temperature (T_e) can be calculated using the ratio of two lines of the same species of the ionization stage as [23]:

$$T_e = \frac{\Delta E}{k_B \ln\left(\frac{\lambda_2 I_2 g_1 A_1}{\lambda_1 I_1 g_2 A_2}\right)} \quad (3)$$

where I, λ, g, A , and E are the total intensity, wavelength, statistical weight, absorption oscillator strength and excitation energy of one of the lines, respectively. Primed quantities are those for the second line. These values for the two lines considered are taken from tables of the National Institute of Standards and Technology (NIST) [14]

The electron temperatures for the three metallic targets were calculated using Eq. (3) from the ratios of the intensities of emission lines. Figure (5) shows that the electron temperature (T_e) increases with increasing laser peak power. The electron temperature is strongly dependent on the laser peak power as the latter is the source of evaporation, atomization and ionization of the target when focused on.

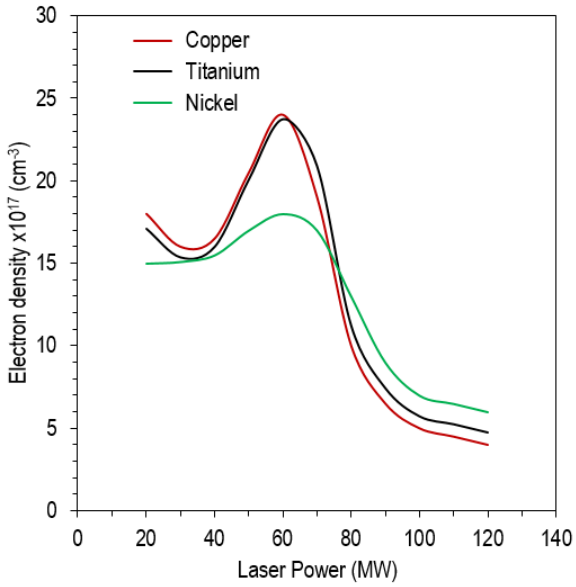

Fig. (4) Variation of electron density of laser-induced plasmas generated in this work with laser peak power

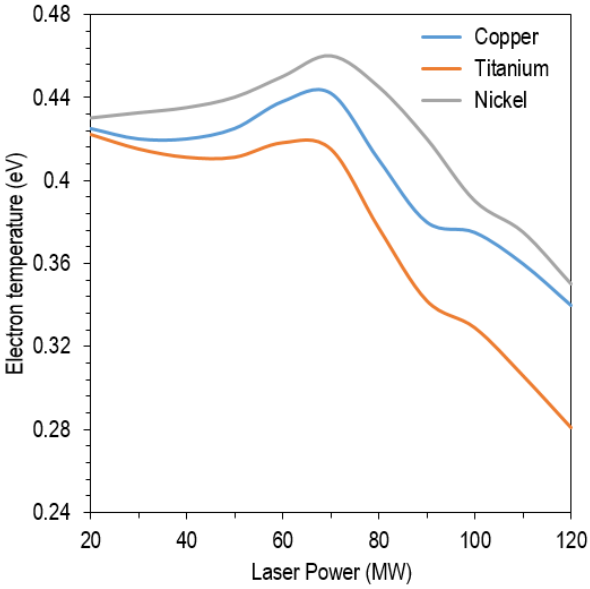

Fig. (5) Variation of electron temperature of laser-induced plasmas generated in this work with laser peak power

4. Conclusion

Three different metallic targets (copper, titanium and nickel) were irradiated by Q-switched Nd:YAG laser pulses to produce transient and elongated plasmas. Measurements of electron density and temperature were carried out by optical emission spectroscopy technique. Line intensity ratios of the

successive ionization stages of the metal target were used for the determination of electron temperature and Stark broadened profile of first ionized tin species was used for the electron density measurements. The dependencies of electron density and electron temperature on different experimental parameters like distance from the target surface were studied. The electron temperatures in the range of 0.34-0.442 eV, 0.281-0.418 eV and 0.35-0.46 eV were obtained for the copper, titanium and nickel plasmas, respectively, while electron densities down to 4x1017 cm^{-3} and up to 23.76x1017 cm^{-3} were observed.

References

[1] S. Palmer and K. Leroy, "Pulsed-laser induced plasma of ionic solids", Appl. Phys. Rep., 14(1) (2000) 39-48.
[2] A.K. Yousif and O.A. Hamadi, "Plasma-induced etching of silicon surfaces," Bulg. J. Phys., 35(3), 191–197, 2008.
[3] R.A. Ismail et al., "Full characterization at 904nm of large area Si p-n junction photodetectors produced by laser-induced diffusion," Int. J. Mod. Phys., 19(31), 197–201, 2007.
[4] O.A. Hammadi and N.E. Naji, "Electrical and spectral characterization of CdS/Si heterojunction prepared by plasma-induced bonding," Opt. Quantum Electron., 48(8), 1–7, 2016. DOI 10.1007/s11082-016-0647-2
[5] R.A.H. Hassan and F.T. Ibrahim, "Preparation and Characterization of Anatase Titanium Dioxide Nanostructures as Smart and Self-Cleaned Surfaces", Iraqi J. Appl. Phys., 16(4) (2020) 13-18.
[6] M.A. Hameed and Z.M. Jabbar, "Preparation and Characterization of Silicon Dioxide Nanostructures by DC Reactive Closed-Field Unbalanced Magnetron Sputtering", Iraqi J. Appl. Phys., 12(4) (2016) 13-18.
[7] E.A. Al-Oubidy and F.J. Al-Maliki, "Photocatalytic activity of anatase titanium dioxide nanostructures prepared by reactive magnetron sputtering technique", Opt. Quantum Electron., 51(1) (2019) 23.
[8] O.A. Hamadi, "Profiling of Antimony Diffusivity in Silicon Substrates using Laser-Induced Diffusion Technique", Iraqi J. Appl. Phys. Lett., 3(1) (2010) 23-26.
[9] T. Dominguez et al., "Optical emission of excited states in laser-produced plasma", Sci. Eng. Rev., 8(6) (2002) 101-112.
[10] S.H. Faisal and M.A. Hameed, "Heterojunction Solar Cell Based on Highly-Pure Nanopowders Prepared by DC Reactive Magnetron Sputtering", Iraqi J. Appl. Phys., 16(3) (2020) 27-32.
[11] F.J. Kadhim and A.A. Anber, "Highly-Pure Nanostructured Silicon Nitride Films Prepared by Reactive DC Magnetron Sputtering", J. Indust. Eng. Sci., 25(5) (2016) 91-94.
[12] M. Arab et al., "Comparison Study of Two Commercial Spectrometers for Heavy Metal Analysis of Laser Induced Breakdown Spectroscopy (LIBS)", Phot. Sens., 4(1) (2014) 63-69.
[13] O.A. Hammadi, M.K. Khalaf and F.J. Kadhim, "Fabrication and characterization of UV photodetectors based on silicon nitride nanostructures prepared by magnetron sputtering," Proc. IMechE Part N: J. Nanoeng. Nanosys., 230(1), 32–36, 2015. DOI: 10.1177/1740349915610600.
[14] J. Keen and D. Monahan, **"Emission Spectroscopy of Laser-Produced Plasmas in Atmospheric Environment"**, Dollhouse Publishing (NY, 2004), 145, 233, 381.
[15] K.S. Khashan and O.A. Hamadi, "Features of spot-matrix surface hardening of low-carbon steel using pulsed laser", Eng. Technol. J., 25(2) (2007).
[16] M.A. Hameed, S.H. Faisal, R.H. Turki, "Characterization of Multilayer Highly-Pure Metal Oxide Structures Prepared by DC Reactive Magnetron Sputtering Technique", Iraqi J. Appl. Phys., 16(4) (2020) 25-30
[17] D.A. Cremers and L. J. Radziemski, **"Handbook of Laser-Induced Breakdown Spectroscopy"**, John-Wiley & Sons, Ltd. (Chichester, 2006).
[18] R.A.H. Hassan and F.T. Ibrahim, "Preparation and Characterization of Ni-doped TiO_2 Nanostructures for Surface Cleaning Applications", Iraqi J. Appl. Phys., 17(1) (2021) 3-8.
[19] O.A. Hamadi and K.Z. Yahiya, "Optical and electrical properties of selenium-antimony heterojunction formed on silicon substrate", Sharjah Univ. J. Pure Appl. Sci., 4(2) (2007) 1-11.
[20] S. Ben Zakour and H. Taleb, "Shift Endpoint Trace Selection Algorithm and Wavelet Analysis to Detect the Endpoint Using Optical Emission Spectroscopy", Phot. Sens., 6(2) (2016) 158-168.
[21] O.A. Hamadi, "Characteristics of CdO-Si Heterostructure Produced by Plasma-Induced Bonding Technique", Proc. IMechE, Part L, J. Mater.: Design & Appl., 222 (2008) 65-71.
[22] F.J. Al-Maliki and E.A. Al-Oubidy, "Effect of gas mixing ratio on structural characteristics of titanium dioxide nanostructures synthesized by DC reactive magnetron sputtering", Physica B: Cond. Matter, 555 (2019) 18-20
[23] A.K. Sharma et al., "Diagnostic technique for determination of ion and electron parameters using plasma spectroscopy", App. Phot. Spect., 9(1) (2014) 69-78.
[24] O.A. Hamadi, "Characterization of SiC/Si Heterojunction Fabricated by Plasma-Induced Growth of Nanostructured Silicon Carbide Layer on Silicon Surface", Iraqi J. Appl. Phys., 12(2) (2016) 9-13.
[25] C. Perez et al., "Detection limit of LIBS for low-ppm heavy metallic elements", Chem. Anal. Appl., 12(8) (2018) 1045-1054.
[26] O.A. Hamadi, B.A.M. Bader and A.K. Yousif, "Electrical Characteristics of Silicon p-n Junction Solar Cells Produced by Plasma-Assisted Matrix Etching Technique", Eng. Technol. J., 28 (2008).
[27] D. Zhong and Z. Li, "Material Measurement Method Based on Femtosecond Laser Plasma Shock Wave", Phot. Sens., 7(1) (2017) 1-10.
[28] O.A. Hamadi, "Effect of Annealing on the Electrical Characteristics of CdO-Si Heterostructure Produced by Plasma-Induced Bonding Technique", Iraqi J. Appl. Phys., 4(3) (2008) 34-37.
[29] H. R. Griem, **"Plasma Spectroscopy"**, McGraw-Hill (NY, 1964).
[30] O.A. Hammadi, M.K. Khalaf and F.J. Kadhim, "Fabrication of UV photodetector from nickel oxide nanoparticles deposited on silicon substrate by closed-field unbalanced dual magnetron sputtering techniques," Opt. Quantum Electron., 47(2), 1–9, 2015. DOI: 10.1007/s11082-015-0247-6
[31] R.H. Turki and M.A. Hameed, "Spectral and Electrical Characteristics of Nanostructured NiO/TiO_2 Heterojunction Fabricated by DC Reactive Magnetron Sputtering", Iraqi J. Appl. Phys., 16(3) (2020) 39-42.
[32] O.A. Hammadi, "Photovoltaic properties of thermally-grown selenium-doped silicon photodiodes for infrared detection applications," Phot. Sens., 5(2), 152–158, 2015. DOI: 10.1007/s13320-015-0241-4
[33] W.L. Wiese and G.A. Martin, "Wavelengths and Transition Probabilities for Atoms and Atomic Ions", Part II, National Bureau of Standards, Washington, DC, (1980).
[34] O.A. Hammadi and M.S. Edan, "Temperature Dependencies of Refractive Index and Optical Elasticity Coefficient on Lens

Induced in Nd:YAG Crystal", Iraqi J. Appl. Phys., 8(1) (2012) 35-41.
[35] M.V. Allmen and A. Blatter, **"Laser-Beam Interaction with Materials: Physical Principles and Applications"**, Springer-Verlag, Berlin, 2nd ed., (1995).
[36] F.J. Al-Maliki, O.A. Hammadi and E.A. Al-Oubidy, "Optimization of Rutile/Anatase Ratio in Titanium Dioxide Nanostructures prepared by DC Magnetron Sputtering Technique", Iraqi J. Sci., 60(special issue) (2019) 91-98.
[37] A.W. Miziolek, V. Palleschi and I. Schechter, **"Laser-induced breakdown spectroscopy: fundamentals and applications"**, Cambridge University Press, 2006.
[38] O.A. Hammadi, "Fabrication of High-Quality Microchannels for Biomedical Applications Using Third-Harmonic Radiation of Nd:YAG Laser", J. Laser Sci. Eng., 10(2) (2018) 61-64.
[39] K. Song, Y., L. Lee and J. Sneddon, "Applications of laser induced breakdown spectrometry," Appl. Spect. Rev., 32(3) (1997) 183-235.

 ISSN (print) 2958-8960 (online) xxxx-xxxx Printed in IRAQ